Chemical routes to materials

Shear exfoliation of large-size GO sheets for high-performance films

Chengjie Weng[1,2], Jian Wu[1], Liming Shen[1,*], and Ningzhong Bao[1,2,*]

[1] State Key Laboratory of Materials-Oriented Chemical Engineering, College of Chemical Engineering, Nanjing Tech University, Nanjing 210009, China

[2] School of Materials Science and Engineering, Zhejiang-California International NanoSystems Institute, Zhejiang University, Hangzhou, Zhejiang 310058, P. R. China

ABSTRACT

Graphene-based film with superior mechanical and conductive performance shows potential applications in the fields of environment and energy. The large-scale production of large graphene oxide (GO) sheets is of great significance to improve the properties of macroscopic films. Here, we show an efficient shear exfoliation method for producing GO with large size and high yield. The size control is based on a size-dependent shear exfoliation pattern, in which the shear rate (γ) required for exfoliation increases with initial size of graphite oxide flakes (L_0) as power law. In this regard, the production of GO with lateral size of 14 μm and relative single-layer fraction of 80% is realized by optimizing γ and L_0. Due to the more compact and oriented structure, the GO film prepared with large GO sheets ($\sim$ 14 μm) exhibits superior tensile strength ($\sim$ 168.2 MPa), Young's modulus ($\sim$ 8.2 GPa), and electrical conductivity ($\sim$ 231.2 S/cm) after HI reduction, which has been increased by 38.8%, 70.8%, and 46.8% than that of GO film prepared with small GO sheets ($\sim$ 3.4 μm), respectively. These findings will be of great value in optimizing size and yield of GO sheets and provide useful information to design shear exfoliation process.

GRAPHICAL ABSTRACT
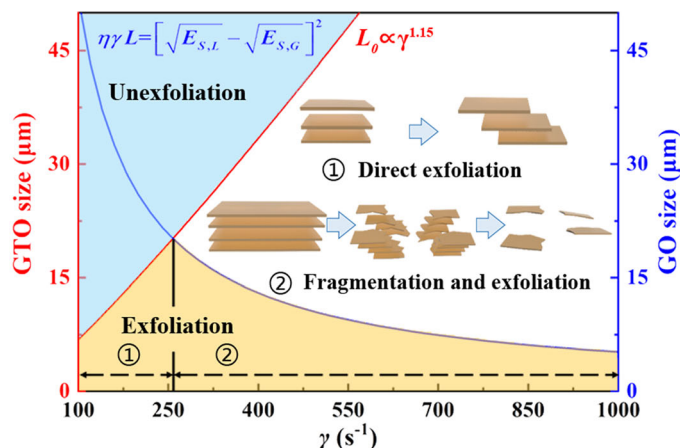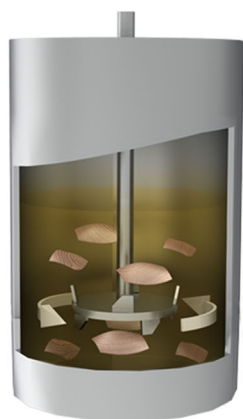
Introduction

As a two-dimensional material, graphene oxide (GO) has attracted tremendous attention due to its excellent properties and potential applications. For example, GO sheets can be assembled into macroscopic films, which is not only an important precursor for large-scale production of graphene film but also a promising material used in the fields of energy and environment [1–5]. The lateral size of the building blocks plays a significant effect on the properties of the films, and large GO sheets with a large basal plane to edge ratio are favorable to high mechanical strength [6, 7], electrical conductivity [8], and thermal conductivity [9, 10]. In this regard, the preparation of GO sheets with large size is required to meet the demands of high-performance films.

Typically, GO sheets can be prepared by the liquid-phase exfoliation of layered graphite oxide (GTO). In the most common sonication method, the constant formation and implosion of vacuum bubbles generate cavitation shear stress and compressive stress in the liquid [11, 12]. However, due to the non-uniform acoustic cavitation, it is difficult to control the shear stress and compressive stress that fragments GTO flakes and results into smaller sheets [13, 14]. The mean size of obtained GO sheets is in the range of hundreds of nanometers to a few micrometers [15].

Although milder sonication method with short periods can produce large GO sheets, they lead to a decrease in relative monolayer fraction and a wide size distribution [16, 17]. Recent papers showed that the sizes of GO sheets and their size distribution can be controlled by size fractionation methods, such as centrifugation, density gradient centrifugation, member-filtration, and pH regulation [7, 18–21]. However, the extremely complex technological processes and time consumption make these techniques unscalable.

Thus far, various shear technologies have been applied to exfoliate 2D materials due to the advantages of operating simplicity and controllable shear stress [22]. Paton et al. [23] established a sliding model to quantitatively describe the effect of shear stress on the exfoliation of 2D materials such as graphite, MoS_2, and BN and reported a minimum shear rate of 10^4 s^{-1} for the exfoliation of graphite. Compared with graphite, GTO flakes have enlarged interlayer spacing due to the intercalated oxygen-containing groups that weaken the van der Waals forces between graphene layers and thus should be easier for shear exfoliation. For example, Jeong et al. [24] used a homogenizer to exfoliate GTO flakes with lateral size of 70 μm at 10,000 RPM for 1 h and obtained GO sheets with a mean size above 10 μm. Park et al. [25] reported the preparation of few-layer

GO with a lateral size of several tens of micrometers by using a Couette–Taylor flow reactor. However, the minimum shear rate for GO exfoliation is still questionable. It will be very useful for the preparation of GO slurry and GO film if we can find out an appropriate shear rate which can fully exfoliate GTO flakes with minimum particle breakage.

In this work, we reported a high-strength GO film utilizing an efficient shear exfoliation method. Within the exfoliation process, GTO flakes with different initial size were exfoliated under various shear rates to shed lights to the effect of shear rate and initial particle size on the exfoliation process. Leveraging the optimized shear rate and the size-dependent exfoliation mechanism, commercially GTO processed by shear exfoliation offers high-quality GO slurry with large size and high concentration (20 g/L). Particularly, the GO slurry prepared from GTO flakes ($\sim$ 20 μm) exfoliated at 700 RPM for 8 h showed the lateral size of 14 μm and relative single-layer fraction of $\sim$ 80%. In addition, the as-prepared GO sheets were assembled and chemically reduced to get the GO and reduced GO (rGO) film. Large GO sheets assembled as more compact films with fewer intersheet junctions, inducing stronger mechanical performance, and higher electrical conductivity.

Experimental

Chemical and materials

Commercial GTO filter cakes (45 wt%) with different lateral sizes were purchased from Zhenjiang Dibo New Material Technology Co. Ltd. According to the lateral size of GTO flakes, GTO solutions used in this work were named as GTO-20 ($\sim$ 20 μm), GTO-30 ($\sim$ 30 μm), GTO-60 ($\sim$ 60 μm), and GTO-90 ($\sim$ 90 μm), respectively (Figure S1). These GTO filter cakes were prepared via a controlled Hummers method by adjusting the mass ratio of $KMnO_4$/graphite. In detail, the mass ratio of $KMnO_4$/graphite was 3.3, and the reaction temperature and time were 55 °C and 2 h, respectively. The oxidation degrees of these GTO flakes were characterized with X-ray photoelectron spectroscopy, and the C/O atomic ratio varied among 2.03, 2.06, 2.18, and 2.24 for GTO-20, GTO-30, GTO-60, and GTO-90, respectively (Figure S2). The results suggested that the oxidation degree increased with the decrease in lateral size.

Ammonium hydroxide (25–28%) was purchased from Shanghai Lingfeng Chemical Reagents Company.

Shear exfoliation of graphite oxide

For a typical preparation of 20 g/L GTO suspension, 88.9 g GTO filter cake was diluted with 1911.1 g DI water followed by a mild mechanical stirring for 30 min. After that, 13.3 mL ammonium hydroxide was slowly added into the suspension to balance the acidity. The suspension was then slowly stirred for another 30 min, so that the GTO flakes were well dispersed in mixture. This pre-mixed suspension (liquid volume V = 500 mL) was then transferred to a stationary mix vessel (inner diameter: 10 cm; outer diameter: 12 cm, tank volume: 2 L) and exfoliated in a high shear mixer. The shear mixing system and its schematic diagram are shown in Figure S3. A saw tooth dispersion plate (Φ = 8 cm) was mounted 3 cm above the bottom of the tank and the liquid height, T, was fixed at 6.4 cm. The shear rate of the liquid in the mixing tank was measured by $\gamma = D\pi N/d$ [23], where D is the diameter of plate and d is the gap between edge of plate and tank wall. The shear rates were 293, 628, 963, 1256, 1591, 1884, and 2219 s^{-1}, corresponding to 700, 1500, 2300, 3000, 3800, 4500, and 5300 RPM, respectively. The temperature of the mixing system was maintained at 20 ± 1 °C with a temperature circulator.

To test the effect of GTO size and shear rate on the exfoliation process, 5 mL of the sample was collected from GTO slurries exfoliated at different shear rates. These slurries were studied by a viscometer and optical measurement to measure the viscosity and yield, respectively. Before optical measurements, the samples were diluted to 0.5 g/L with DI water followed by centrifugation at 4000 RPM for 15 min, so that the mono- and few-layer GO sheets dispersed in the supernatant would be separated from un-exfoliated GTO flakes. The obtained GO solutions were then diluted by the factors of 5–20, and their concentration was determined by standard curve method according to Lambert–Beer law ($A = Kbc$, Figure S4) [25–27]. The relative monolayer fraction α was calculated quantitatively by comparing the GO concentration in supernatant (C_i) and initial concentration of GTO (C_o), by $\alpha = C_i/C_o$. This value also represents the yield of GO sheets.

Preparation of GO and rGO films

Blade-coating technology was introduced to prepare GO films. The GO slurry was firstly coated on a polyethylene glycol terephthalate (PET) substrate by an automatic coating machine, and the gap of casting blade was fixed at 1 mm. After drying at 40 °C in an oven for 6 h, the paper-like GO film was peeled off from the substrate. The as-prepared GO films were reduced by immersing them in mixture of HI acid and acetic acid (AcOH) (volume ratio = 1:1) in a hydrothermal reactor, which was then heated at 80 °C for 12 h. The reduced GO (rGO) films were repeatedly washed with ethanol and deionized water and finally dried at 60 °C for 12 h. The fabrication process is shown in Fig. 1.

Characterization

The morphologies of GTO flakes processed before and after shear exfoliation were measured by optical microscope (OM) (Model BM2000, China). These obtained OM images were then analyzed by a commercial image analysis software ImageJ to determine the sheet area (S). To obtain their lateral size (L) from area data, we assumed that GTO flakes and GO sheets were quadrangles, and L was then calculated by the log-normal fitting of the side length ($\sqrt{S}$) distribution histograms, which represented most probable length of these sheets [28, 29]. Similarly, the morphology of exfoliated GO sheets was studied by scanning electron microscopy (SEM) (Model S4800, Hitachi, Japan) with an accelerated voltage of 5 kV followed by the above statistical analysis on the lateral size (L') of GO sheets. The thickness of GO sheets was studied by atomic force microscope (AFM) (Model Autoprobe CP-Research, Bruker, USA). X-ray photoelectron spectroscopy (XPS) (Model PHI-5000 Versaprobe III, Ulvac-Phi, Japan) was used to measure the C/O ratio of samples. The structures of GO

and rGO films were examined by X-ray diffraction (XRD) (Model Rigaku SmartLab SE, Japan) and Raman spectroscopy (Model Labram HR800, Horiba Jobin, France). Viscosity measurements were taken by using a viscometer (Model DV2TRV, Brookfield, USA) with a CAP-51Z cone spindle at 20 °C (cone angle: 1.5°, cone radius: 1.2 cm, sample volume: 0.5 mL), where the shear rate was adjusted from 100 to 750 s^{-1}. The ultraviolet–visible spectrometer (UV–Vis) (Model Cray 5000, Agilent, USA) was used to measure the absorbance of GO dispersion at 231 nm. Samples for optical measurement were diluted below 0.1 g/L, followed by pre-treatment by sonication for 30 min to prevent the influence of GO size on absorbance. Mechanical property tests were carried out on a tensile testing machine (Model KJ-1065, China) with a loading rate of 2 mm/min and a gauge distance of 1 cm. Electrical conductivity was measured with a four-probe apparatus (Model RTS9, China).

Results and discussion

Shear exfoliation of graphite oxide

The key advantage of shear exfoliation technology lies in the controlled shear rate and shear stress in the mixture [30]. In order to obtain the required shear rate for the shear exfoliation of GTO, we used a series of shear rates to exfoliate GTO-90 and the GO yield in slurry was characterized by UV–vis spectroscopy. As indicated by the UV–Vis absorption spectra shown in Fig. 2a, all the diluted GO supernatants have absorbance at 231 nm, which is attributed to the $\pi \to \pi^*$ transitions of C–C bonds, while the samples collected from the GTO-90 slurries those were exfoliated at the shear rates of 293 and 628 s^{-1} exhibit relatively low absorbance. As the shear rate increases to 963 s^{-1}, there is a significant increase in absorbance (blue line)
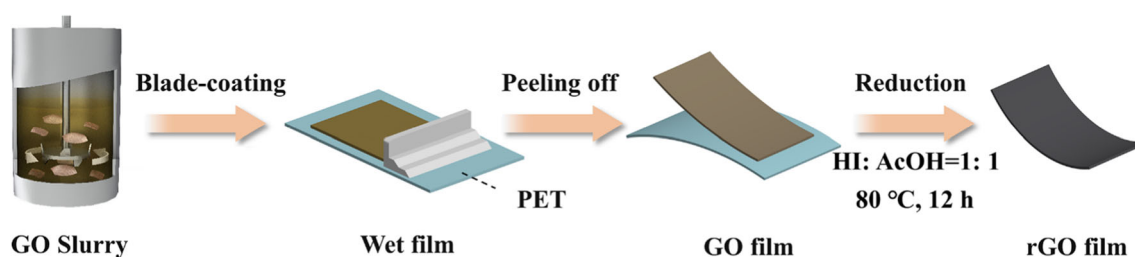
Figure 1 Schematic illustration of preparing GO and rGO films.
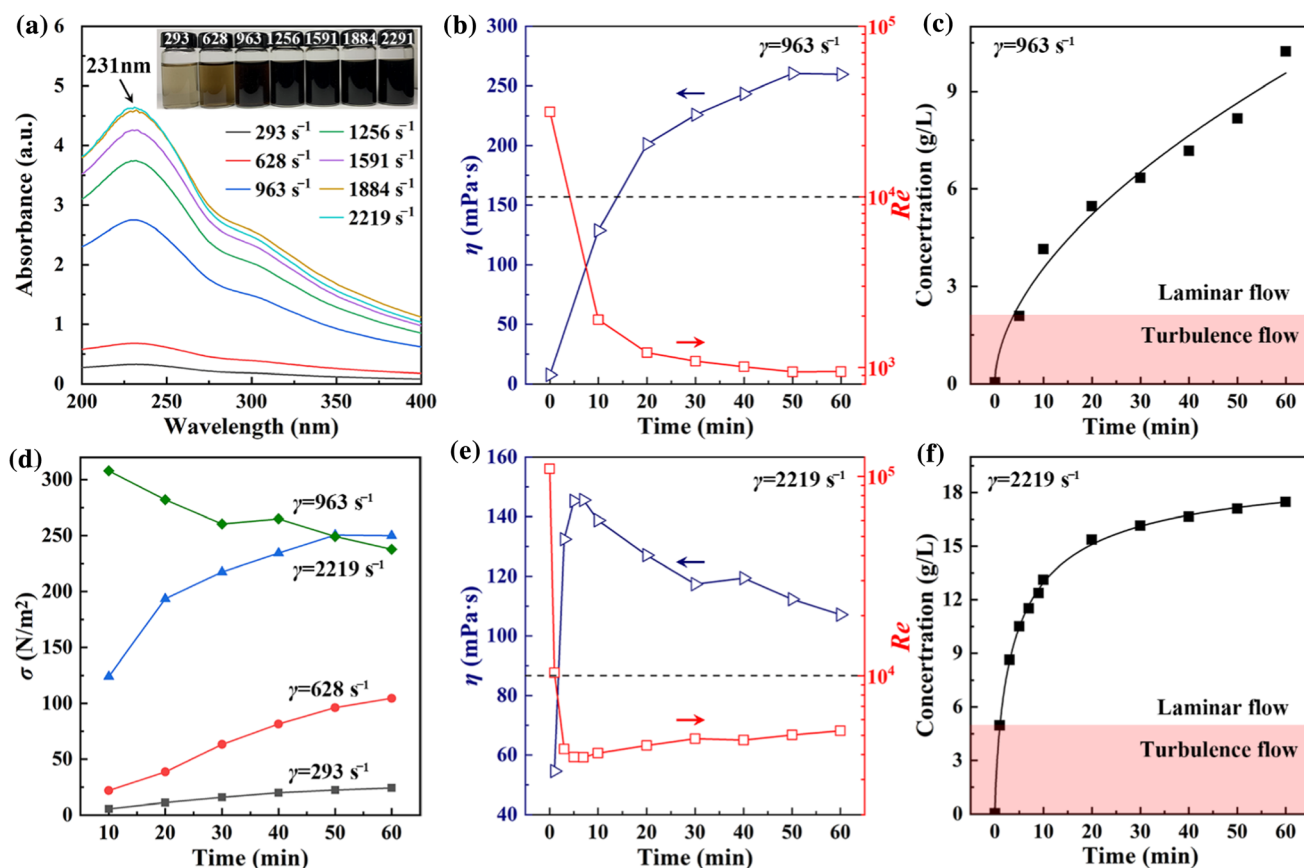
Figure 2 Effect of shear rate on the exfoliation of GTO-90. **a** UV–Vis spectra of the diluted supernatants collected from the GTO-90 slurries after exfoliation at different shear rates for 1 h. The inset shows the color change of these supernatants. Evolution of viscosity and Reynolds number (*Re*) of GTO slurry exfoliated at shear rate of **b** 963.0 and **e** 2219.0 s^{-1}. The viscosity was predicted according to the power law viscosity model (Figure S6). **c − f** Time-dependent concentration of the supernatant collected from the GTO-90 slurry exfoliated at **c** 963.0 s^{-1} and **f** 2219.0 s^{-1}. **d** Shear stress of GTO slurries under different shear conditions.

and the concentration of corresponding GO supernatant is calculated to be 10.23 g/L based on the standard curve (Figure S5), which clearly reflects that the minimum shear rate for GTO-90 is 963 s^{-1}.

To obtain quantitative information about the shear stress acting on the flake surface, in this work, we measured the viscosity in different fluid flow situations and predicted the flow patterns by Reynolds number (*Re* = $ND^2\rho/\eta$) [23], where *N* is the agitation speed, *D* is the diameter of the saw disk, and ρ and η are the density and viscosity of the fluid, respectively. At low Reynolds numbers (*Re* < 10,000), flow patterns are dominated by laminar (sheet-like) flow, while at high *Re* flows tend to be turbulent. Figure 2b shows the variation of viscosity and *Re* of the GTO slurry which was exfoliated at the shear rate of 963.0 s^{-1}. In Fig. 2b, the viscosity increases with the shear time, indicating the on-going exfoliation of GO

sheets; meanwhile, *Re* quickly drops from ~ 30,000 to ~ 1000, implying that the turbulence flow plays a dominant role at the beginning of exfoliation process and then rapidly turns into the laminar flow. At a higher shear rate of 2219 s^{-1} (Fig. 2e), the viscosity of GTO slurry is lower than that obtained at 963 s^{-1}, but still enough to give a *Re* within the laminar flow regime. It is noteworthy that for the GTO-90 slurries exfoliated at both shear rates, their GO supernatants collected from the turbulent regimes are relatively lower in concentration (Fig. 2c, f), suggesting that the GO sheets were peeled off under the laminar flow. The above results infer that for the GTO slurries exfoliated at a shear rate in range of 963–2219 s^{-1}, the exfoliation of GTO is controlled by the laminar flow. For a laminar flow, the shear stress (σ) can be calculated by using Newton's law [23], $\sigma = \eta\gamma$. The time-dependent σ values under different shear rates are

shown in Fig. 2d. We can clearly observe a significant increase in σ when the shear rate rises from 628 to 963 s^{-1}, providing a strong shear stress for the GTO exfoliation.

Shear exfoliation mechanism

The effect of shear stress can be further revealed by the exfoliation model. Like other two-dimensional materials, the exfoliation of GTO can be treated as shear-induced interlayer sliding, during which the relative sliding of GO layers results in shear delamination and the interfacial bonding energy changes with the movement of sheets [31]. The energy change on delamination (ΔE) can be calculated by [23]:

$$\Delta E = L^2 \left[\sqrt{E_{S,L}} - \sqrt{E_{S,G}} \right]^2 \tag{1}$$

where L is the flake size and $E_{S,G}$ and $E_{S,L}$ are surface energies of GTO and DI water ($E_{S,L}$ = 72.8 mJ/m^2, 20 °C), respectively. When the surface delamination energy induced by shear stress ($E_D = \eta\gamma L^3$) matches the interfacial energy of GTO flakes, they are exfoliated to mono- and few-layer GO sheets. In such cases, Eq. 1 can be rewritten as

$$\eta\gamma L = \left[\sqrt{E_{S,L}} - \sqrt{E_{S,G}} \right]^2 \tag{2}$$

This formula reveals the relationship between the operating parameters of shear exfoliation and the basic features of GTO flakes.

The flake size in delamination stage was measured by SEM analysis and its size distribution was determined based on the statistical analysis over 100 sheets. As shown in Fig. 3a, the size distribution of GO sheets exfoliated at 963 s^{-1} for 1 h from GTO-90 flakes is in range of around 2 to 13 μm. And the most probable lateral size of GO sheets, L', is about 5.8 μm which is much smaller than the initial size ($\sim$ 90.0 μm). This result indicates that GTO-90 prefers to fracture into several smaller particles due to the local turbulence and the impact force generated around the rotating blade (Figure S7) [14, 32]. Besides, from the curve of GO concentration in supernatant versus shear time (Fig. 2c), we found that the shear exfoliation accelerated at the shear time of about 10 min, but the viscosity did not reach its maximum value at this point. This result clearly indicates that it is the shear rate that plays a dominant function in the shear exfoliation, and the

increase in viscosity in the early stage of exfoliation is mainly associated with the fragmentation of flakes. We can presume that the viscosity will increase rapidly once mass delamination of flakes starts off. Thus, we regard the moment of 10 min as the beginning of shear exfoliation where the viscosity is 128.8 mPa·s. By substituting L' = 5.8 μm, γ = 963 s^{-1}, and η = 128.8 mPa·s into Eq. 2, the surface energy is calculated to $E_{S,G} \approx$ 59.0 mJ/m^2, which is close to the reported value (62.1 mJ/m^2) [33].

It is worth noting that these GTO-90 flakes are supposed to have similar surface energy. Figure 3b shows the XPS spectra of above GO sheets. For GO slurry exfoliated at 293 s^{-1}, its C/O atomic ratio is 3.31, and the compositions of C = C/C-C, C-O, and C = O are 58.9%, 36.1%, and 5.0%, respectively (Figure S8a). When the shear rate increases to 963 and 2219 s^{-1}, the C/O atomic ratio changes to 3.01 and 2.98, and the compositions of C = O reach 8.1% and 7.9%, respectively. The slight increase in C/O atomic ratio is associated with the content of carboxyl groups at the edge of GO sheets (Figure S8b,c). Besides, the similar C/O atomic ratios and chemical compositions of the latter two samples indicate that they have similar oxidation degree. It can be further confirmed with FT-IR analysis. In Figure S8d, there are no obvious changes between FT-IR spectra of GO exfoliated at 963 and 2219 s^{-1}. These results clearly reflect that the influence of oxidation degree on the surface energy is negligible. By substituting $E_{S,G} \approx$ 59.0 mJ/m^2 and η = 128.8 mPa·s into Eq. 2, an estimation curve was obtained to predict the lateral size of well-exfoliated GO product at a given γ. As shown in Fig. 3c, the measured lateral sizes of GO products obtained from different shear rates are in good agreement with the estimation curve, indicating that the GO size decreases with shear rate.

To prevent the sheets breakage under high shear force, a mild shear condition is necessary. Considering the geometry of GTO flakes, large flakes tend to be thicker and requires more energy to break up and exfoliate than small ones [34]. In this regard, smaller GTO flakes (GTO-60, GTO-30, and GTO-20) are expected to exfoliate at low shear rates to avoid the sheet breakage. As shown in Fig. 3d, at a low shear rate (γ = 293 s^{-1}), only GTO-20 flakes could be exfoliated, indicated by a significant increase in GO concentration, while GTO-30, GTO-60, and GTO-90 all gave a low concentration at this agitation speed. It is worth noting that the yield of GO sheets increases
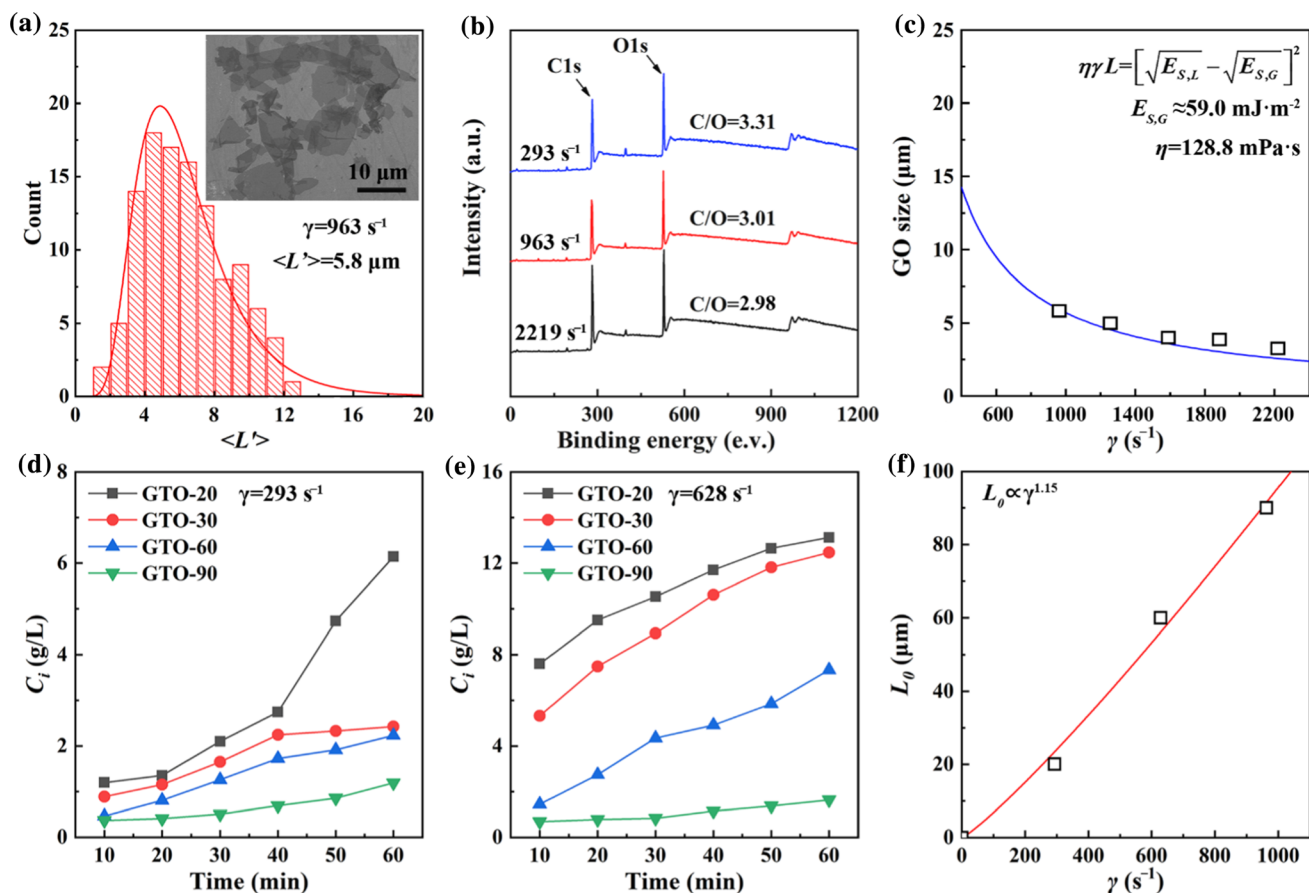
Figure 3 a Statistical distribution of lateral size of GO sheets in supernatant collected from GTO-90 slurry after 60-min exfoliation with a shear rate of 963 s^{-1}. Inset picture shows the corresponding SEM image of GO sheets. **b** XPS survey of GO slurry exfoliated at 293, 963, and 2219 s^{-1} for 1 h. **c** Estimated and measured lateral sizes of GO sheets exfoliated from GTO-90 plotted versus shear rate. The solid line is a fit to Eq. 2, and the hollow blocks represent the experimental value obtained from SEM images. **d, e** GO concentration in supernatant collected from GTO slurry with initial sizes of about 20, 30, 60, and 90 μm exfoliated at shear rates of **d** 293 and **e** 628 s^{-1}. **f** The effect of initial size of GTO flakes on required shear rate for exfoliation. The line is the fitting result of $L_0 = 0.035\gamma^{1.15}$.

with the shear time and reaches ∼ 80% after 8-h exfoliation, showing the effective exfoliation of GTO-20 (Figure S9). When the shear rate increased to 628 s^{-1}, both GTO-30 and GTO-60 flakes were able to be exfoliated, and their yields increased with shear time as well (Fig. 3e). It is very interesting that these results clearly reveal a size-dependent exfoliation pattern, where the relationship between the shear rate required for exfoliation and the initial size of GTO flakes fits the power law: $L_0 = 0.035\gamma^{1.15}$ (Fig. 3f).

Thus, both the GTO size and the shear rate need to be taken into account to assess the exfoliation. Once a low shear rate matches the energy requirement for exfoliating small GTO flakes, it can not only lead to a direct exfoliation process where the GO sheets

exfoliate from the mother flakes layer by layer, but also prevent the particle breakage. As for GTO-20, the lateral size of GTO-20 chips collected from precipitate decreased with the shear rate rising from 293 to 628 s^{-1} (Figure S10). At 293 s^{-1}, the calculated L of GTO chips using their optical images was about 20.7 ($t = 20$ min), 20.1 ($t = 40$ min), and 19.4 μm ($t = 60$ min), respectively, which are quite comparable with their initial size (20.9 μm, Figure S1a). In addition, the corresponding GO sheets collected from the GTO-20 supernatant gave an average size of about 14 μm measured from SEM images, indicating a small change in the lateral size occurred over the exfoliation process (Figure S11a). When GTO-20 was exfoliated at 628 s^{-1}, L extracted from optical images was significantly reduced to 12 μm, while the GO size

was about 9.1 μm (Figure S11b). Interestingly, we found the lateral sizes of GO products (L' = 9.1 μm at 628 s^{-1}; L' = 14.0 μm at 293 s^{-1}) prepared with GTO-20 are close to those prepared with GTO-90 at the same shear rates (L' = 8.4 μm at 628 s^{-1}; L' = 14.0 μm at 293 s^{-1}, Figure S11c, d), suggesting that Eq. 2 and the power law model ($L_0 = 0.035\gamma^{1.15}$) are applicable to GTO-20 as well. Based on the above discussion, two possible exfoliation mechanisms with both the GTO size and shear rate being considered are presented in Fig. 4, which discloses the shear rate required for exfoliation and the resulting lateral size of GO sheets. In Fig. 4, we can easily locate a region where a GO slurry with relatively large size and high yield can be obtained. Therefore, this study provides a scalable method to prepare GO dispersion with tunable size and high yield by shear exfoliation with optimum γ and L_0, which exhibits superior size regulation for high-concentration GO slurry. (A comparison is shown in Tables S1 and S2.)

GO slurry and films

On the basis of exfoliation mechanism, we show the successful production of GO with tunable size through shear exfoliation method. As the GO size depends greatly on the shear stress, a high shear rate is desired for preparing small GO sheets. In our experiment, the GO slurry with a lateral size of ∼ 3.4 μm (SGO, Fig. 5a) was obtained by exfoliating GTO-90 at 2219 s^{-1} for 1 h, which exhibited a yield of ∼ 85% (Figure S12). In contrast, GTO-20 was selected as raw materials and exfoliated at 293 and 628 s^{-1} to obtain other two portions with larger sizes.

It is worth noting that the lower shear rate resulted in a decreased input energy, which gave rise to the increase in shear time for complete exfoliation. The shear time of 240 and 480 min was required for GTO-20 exfoliated at 293 and 628 s^{-1} to reach a yield of ∼ 80% (Figure S12), and the GO sizes were about 8.1 (MGO) and 14.0 μm (LGO), respectively (Fig. 5a). To demonstrate the effectiveness of shear exfoliation, the thickness of GO sheets was measured by AFM analysis. Because of the presence of oxygen-containing functional groups, the GO sheets showed a higher thickness than that of graphene (0.335 nm) [35]. The GO sheets had a thickness ranging from 1.0 to 1.4 nm (Fig. 5b), which clearly indicates that these sheets consist of a single layer of GO [36].

The size effect is also reflected by the solution property between the GO slurries described above. The exfoliation process of GTO flakes is accompanied by a rapid volume expansion, which increases the flow resistance of slurry. Hence, well-exfoliated GO slurry performs a typical gelation behavior (Figure S13a). The viscosities of GO slurries were tested by a viscometer in this experiment. Owing to the strongly limited mobility of larger GO sheets [37], LGO has a higher viscosity (365.0 mPa s) than that of MGO (344.9 mPa s) and SGO (288.5 mPa s) (Figure S13b). In addition, the enhanced solution viscosity makes these GO slurries great candidates for GO films via blade-coating technology [38, 39]. After drying completely in an oven, the paper-like large GO films were obtained after being peeled off from substrates. The SEM image (Fig. 6a) reveals that these GO films possess close-packed features.
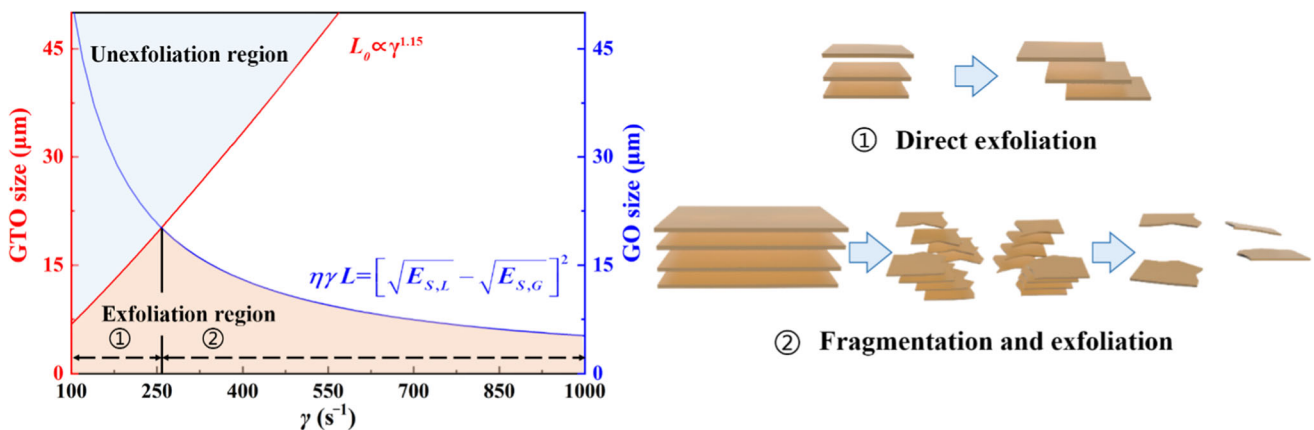
Figure 4 Schematic of exfoliation paths: (1) direct shear exfoliation of small GTO flakes at low γ; or (2) fragmentation and exfoliation of large flakes at high γ.
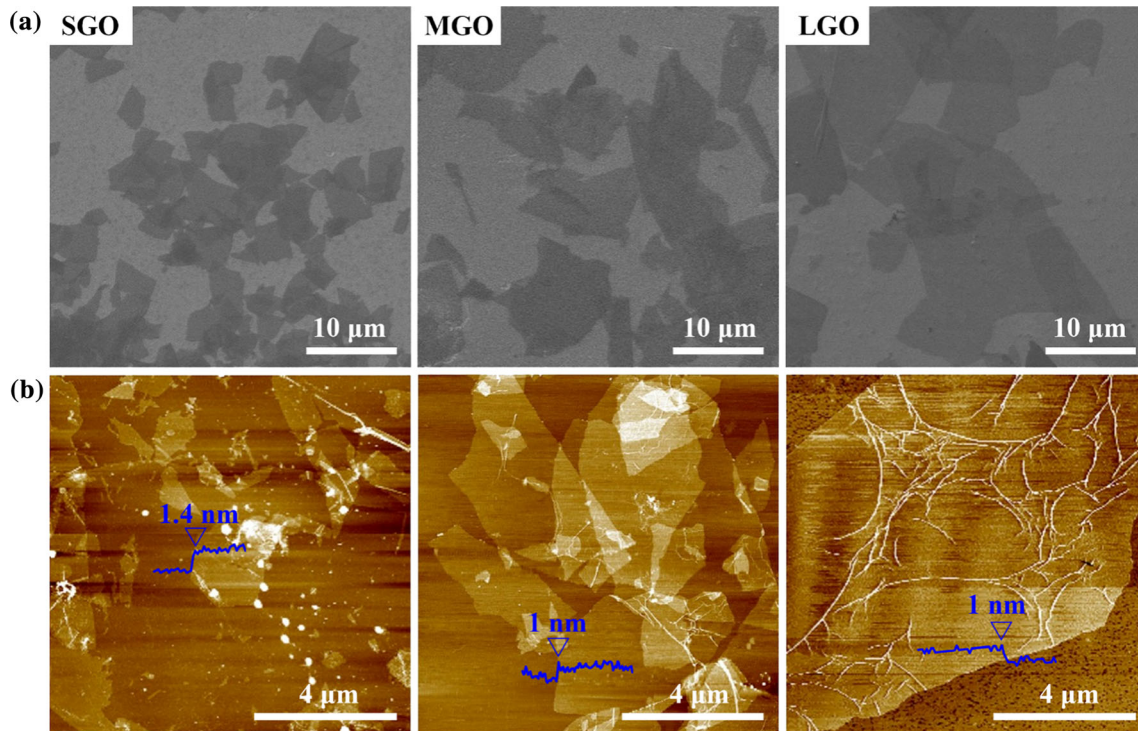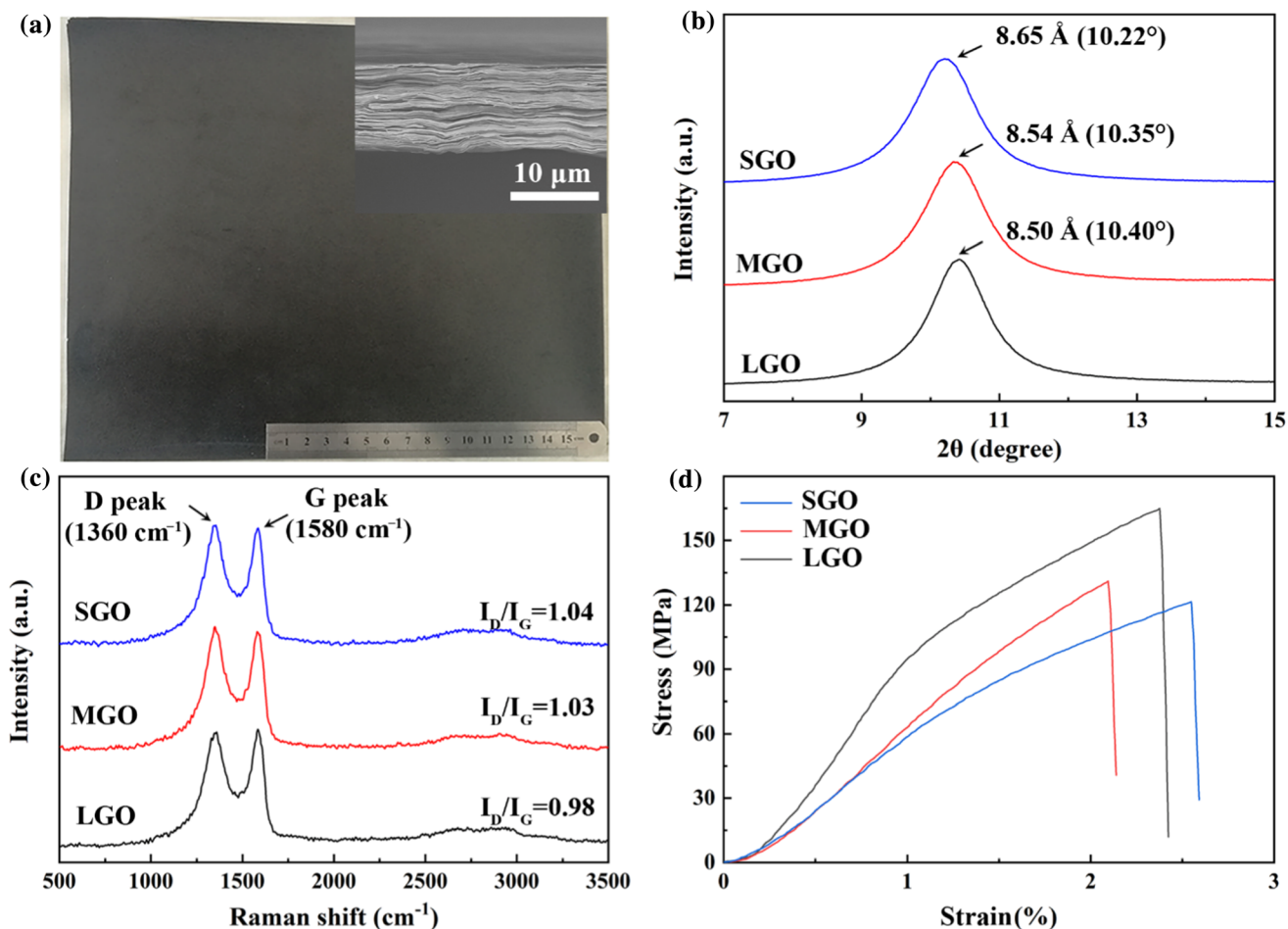
Figure 5 **a** SEM images and AFM images of SGO, MGO, and LGO. The thickness of GO sheets ranges from 1 to 1.4 nm that indicates the single layer of GO.

The structures and properties of GO films are highly dependent on the lateral sizes of their GO sheets. In the XRD patterns of GO films prepared with SGO, MGO, and LGO (Fig. 6b), the peaks centered at $2\theta = 10.22°$, $10.35°$, and $10.40°$, corresponding to the d-spacings of 8.65, 8.54, and 8.50 Å, respectively. The decreased interlayer spacing with the increase in GO size can be attributed to that the smaller GO with higher oxygen content can absorb more water through hydrogen bonding and give rise to an increased d-spacing than that of LGO films [40]. In addition, the full widths at half maximum (FWHM) of these peaks showed a falling trend, namely 1.11°, 1.08°, and 0.99° for SGO, MGO, and LGO films, respectively, which clearly reflected a more orderly alignment of LGO films [30]. The Raman spectra of SGO, MGO, and LGO films were analyzed to indicate the defects in the structure. As shown in Fig. 6c, all samples have two characteristic peaks of D and G emerging at ~ 1350 and ~ 1580 cm^{-1}, corresponding to the defects and sp^2 hybridized region, respectively [41, 42]. The values of intensity ratio, I_D/I_G, vary as 1.04, 1.03, and 0.98 for SGO, MGO, and LGO films, respectively, which reveals fewer defects caused by edge

boundaries in LGO sheets [40]. Figure 6d shows the stress–strain curves of above GO films. It was found that the tensile stress and Young's modulus of GO films increased with lateral size of GO sheets. The SGO film shows a tensile stress of ~ 121.1 MPa and a Young's modulus of 4.8 GPa, while those of LGO film was tested to be ~ 168.2 MPa and 8.2 GPa. The remarkable enhancement in tensile stress and Young's modulus is mainly due to the more compact and oriented structure, fewer defects and inter-sheet junctions in LGO films [7].

The successful size control also provides a possible method to prepare highly conductive graphene films. After reduction by HI, the SGO, MGO, and LGO films were efficiently converted to rGO films. The XRD patterns exhibit characteristic peaks at $2\theta = 24.17°$, 24.24°, and 24.33° for reduced SGO (rSGO), MGO (rMGO), and LGO (rLGO) films, and their d-spacings are measured to be 3.68, 3.67, and 3.66 Å, respectively (Fig. 7a). The significant reduction of interlayer spacing indicates the removal of oxygen-containing functional groups. In addition, from the Raman spectra of rGO films, the intensity of D peak is stronger than that of G peak and a new peak of 2D peak emerges at 2680 cm^{-1}, indicating the recovery

Figure 6 **a** Photograph of a typical LGO film prepared by using blade-coating method. Inset picture shows the corresponding cross-sectional SEM images. **b** XRD patterns, **c** Raman spectra, and **d** stress–strain curves of SGO, MGO, and LGO films.

of the graphitic structures with defects, which results in the stacking of rGO sheets (Fig. 7b) [43]. To relate GO size with the electrical properties, we measured the electrical conductivity of rGO films at 49 points in a 3×3 cm^2 region. As shown in Fig. 7c, all films exhibit uniform conductivity distribution and give mean values of 157.5, 177.1, and 231.2 S/cm for rSGO, rMGO, and rLGO films, respectively. The improvement of conductivity is mainly due to the lower inter-sheet contact resistance of larger sheets. The comparison not only clearly validates the significance of the initial size of GTO to the properties of GO and rGO films, but also demonstrates the high efficiency of our developed exfoliation methodology.

Conclusions

The shear exfoliation of GTO flakes has been systematically investigated, and the major findings and results are listed as follows:

1. A size-dependent exfoliation pattern has been identified for the shear exfoliation of GTO flakes. The relationship between the shear rate (γ) and lateral size of GTO flakes (L_0) was determined to be $L_0 \propto \gamma^{1.15}$ for our high shear mixer system; therefore, GO slurry with high yield can be easily produced by controlling the shear rate in the high shear mixer.

2. In the shear exfoliation of GTO flakes, there are two exfoliation paths: (1) direct shear exfoliation of small GTO flakes at low γ and (2) fragmentation and delamination of large flakes at high γ. In this regard, GO dispersion with tunable size ($\sim 3 - 14$ μm) and high yield can be prepared by shear exfoliation with optimized γ and L_0.
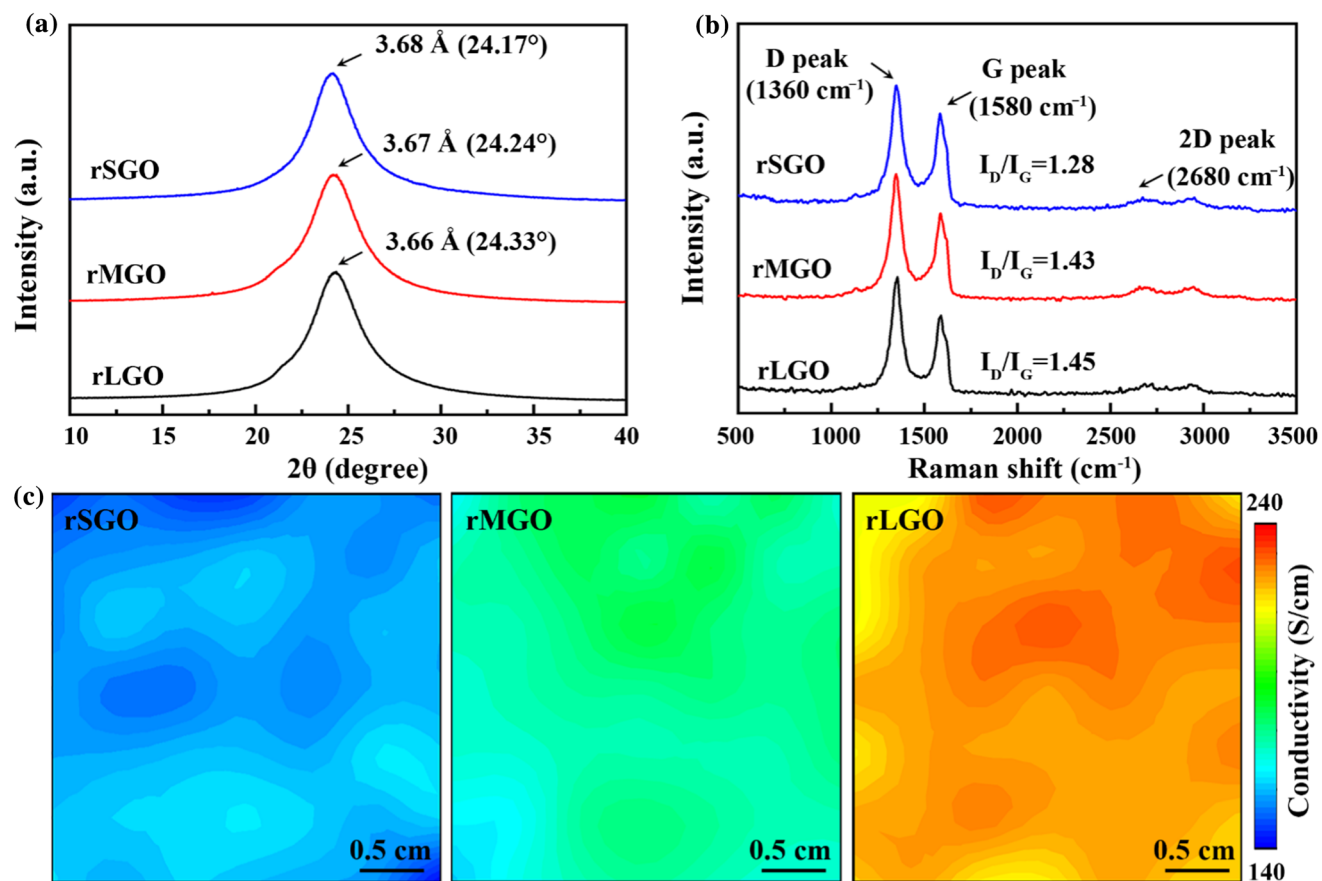
Figure 7 **a** XRD patterns and **b** Raman spectra of rSGO, rMGO, and rLGO films. **c** Multipoints (7 × 7 points) electrical conductivity measurements of rSGO, rMGO, and rLGO films by using four-probe technology. The conductivity distributions are 147 − 164, 172 − 188, and 219 − 240 S/cm for rSGO, rMGO, and rLGO films.

3. The obtained GO slurry shows excellent solution property that can be conveniently transformed to GO film. The LGO film exhibits obvious enhancement in tensile strength (∼ 168.2 MPa), Young's modulus (∼ 8.2 GPa), and electrical conductivity (∼ 231.2 S/cm) after HI reduction, validating the effect of lateral size on the structure and properties of films.

Declarations

Conflict of interests The authors declare that they have no known competing financial interests or personal relationships that could have appeared to influence the work reported in this paper.

Supplementary Information: The online version contains supplementary material available at http s://doi.org/10.1007/s10853-021-06504-x.

References

[1] Chang J, Zhang M, Zhao Q, Qu LT, Yuan JY (2021) Ultratough and ultrastrong graphene oxide hybrid films via a polycationitrile approach. Nanoscale Horiz 6:341–347

[2] Chen SJ, Wang QL, Zhang MM, Huang RZ, Huang YY, Tang J, Liu J (2020) Scalable production of thick graphene films for next generation thermal management applications. Carbon 167:270–277

[3] Yang G, Yi HK, Yao YG, Li CW, Li Z (2020) Thermally conductive graphene films for heat dissipation. ACS Appl Nano Mater 3:2149–2155

[4] Wei W, Guan TX, Li C, Shen LM, Bao NZ (2020) Heating rate-controlled thermal exfoliation for foldable graphene sponge. Ind Eng Chem Res 59:2946–2952

[5] Li J, Chen XY, Lei R-B, Lai JF, Ma TM, Li Y (2019) Highly thermally conductive graphene film produced using glucose under low-temperature thermal annealing. J Mater Sci 54:7553–7562. https://doi.org/10.1007/s10853-019-03406-x

[6] Lin JH, Li P, Liu YJ, Wang Y, Ming X, Gao C, Xu Z (2021) The origin of the sheet size predicament in graphene macroscopic papers. ACS Nano 15:4824–4832

[7] Chen J, Li YR, Huang L, Jia N, Li C, Shi GQ (2015) Size fractionation of graphene oxide sheets via filtration through track-etched membranes. Adv Mater 27:3654–3660

[8] Zhao JP, Pei SF, Ren WC, Gao LB, Cheng HM (2010) Efficient preparation of large-area graphene oxide sheets for transparent conductive films. ACS Nano 4:5245–5252

[9] Huang P, Li Y, Yang G, Li ZX, Li YQ, Hu N, Fu SY, Novoselov KS (2021) Graphene film for thermal management: a review[J]. Nano Mater Sci 3:1–16

[10] Peng L, Xu Z, Liu Z, Guo Y, Li P, Gao C (2017) Ultrahigh thermal conductive yet superflexible graphene films. Adv Mater 29:1700589

[11] Zhu YW, Stoller MD, Cai WW, Velamakanni A, Piner RD, Chen D, Ruoff RS (2010) Exfoliation of graphite oxide in propylene carbonate and thermal reduction of the resulting graphene oxide platelets. ACS Nano 4:1227–1233

[12] Tung VC, Allen MJ, Yang Y, Kaner RB (2009) High-throughput solution processing of large-scale graphene. Nat Nanotech 4:25–29

[13] Brisebois PP, Siaj M (2020) Harvesting graphene oxide-years 1859 to 2019: a review of its structure, synthesis, properties and exfoliation. J Mater Chem C 8:1517–1547

[14] Yi M, Shen ZG (2015) A review on mechanical exfoliation for the scalable production of graphene. J Mater Chem A 3:11700–11715

[15] Kim JH, Sin DH, Kim H, Jo SB, Lee H, Han JT, Cho K (2019) Improved charge transport and reduced non-geminate recombination in organic solar cells by adding size-selected graphene oxide nanosheets. ACS Appl Mater Inter 11:20183–20191

[16] Botas C, Pérez-Mas AM, Álvarez P, Santamaría R, Granda M, Blanco C, Menéndez R (2013) Optimization of the size and yield of graphene oxide sheets in the exfoliation step. Carbon 63:576–578

[17] Ye S, Feng J (2016) The effect of sonication treatment of graphene oxide on the mechanical properties of the assembled films. RSC Adv 6:39681–39687

[18] Sun XM, Luo DC, Liu JF, Evans DG (2010) Monodisperse chemically modified graphene obtained by density gradient ultracentrifugal rate separation. ACS Nano 4:3381–3389

[19] Kumar P, Shahzad F, Yu S, Hong SM, Kim YH, Koo CM (2015) Large-area reduced graphene oxide thin film with excellent thermal conductivity and electromagnetic interference shielding effectiveness. Carbon 94:494–500

[20] Wang XL, Bai H, Shi GQ (2011) Size Fractionation of graphene oxide sheets by ph-assisted selective sedimentation. J Am Chem Soc 133:6338–6342

[21] Lee KE, Kim JE, Maiti UN, Lim J, Hwang JO, Shim J, Oh JJ, Yun T, Kim SO (2014) Liquid crystal size selection of large-size graphene oxide for size-dependent n-doping and oxygen reduction catalysis. ACS Nano 8:9073–9080

[22] Cai CJ, Sang NN, Shen ZG, Zhao XH (2017) Facile and size-controllable preparation of graphene oxide nanosheets using high shear method and ultrasonic method. J Exp Nanosci 12:247–262

[23] Paton KR, Varrla E, Backes C et al (2014) Scalable production of large quantities of defect-free few-layer graphene by shear exfoliation in liquids. Nat Mater 13:624–630

[24] Jeong SY, Kim SH, Han JT, Jeong HJ, Yang S, Lee GW (2011) High-performance transparent conductive films using rheologically derived reduced graphene oxide. ACS Nano 5:870–878

[25] Park WK, Yoon Y, Song YH, Choi SY, Kim S, Do Y, Lee J, Park H, Yoon DH, Yang WS (2017) High-efficiency exfoliation of large-area mono-layer graphene oxide with controlled dimension. Sci Rep 7:16414

[26] Yoon HJ, Lee JY, Yoon TH (2018) Millstone exfoliation: a true shear exfoliation for large-size few-layer graphene oxide. Nanoscale Res Lett 13:186

[27] Ogino I, Yokoyama Y, Iwamura S, Mukai SR (2014) Exfoliation of graphite oxide in water without sonication: bridging length scales from nanosheets to macroscopic materials. Chem Mater 26:3334–3339

[28] Kouroupis-Agalou K, Liscio A, Treossi E, Ortolani L, Morandi V, Pugno NM, Palermo V (2014) Fragmentation and exfoliation of 2-dimensional materials: a statistical approach. Nanoscale 6:5926–5933

[29] Ji LJ, Qin Y, Gui D, Li W, Li YC, Li XD, Lu PX (2018) Quantifying the exfoliation ease level of 2d materials via mechanical anisotropy. Chem Mater 30:8732–8738

[30] Afshar Ghotli R, Raman AAA, Ibrahim S, Baroutian S (2013) Liquid-liquid mixing in stirred vessels: a review. Chem Eng Commun 200:595–627

[31] Chen X, Dobson JF, Raston CL (2012) Vortex fluidic exfoliation of graphite and boron nitride. Chem Commun 48:3703–3705

[32] Marchisio DL, Soos M, Sefcik J, Morbidelli M (2006) Role of turbulent shear rate distribution in aggregation and breakage processes. AIChE J 52:158–173

[33] Wang SR, Zhang Y, Abidi N, Cabrales L (2009) Wettability and surface free energy of graphene films. Langmuir 25:11078–11081

[34] Backes C, Campi D, Szydlowska BM, Synnatschke K, Ojala E, Rashvand F, Harvey A, Griffin A, Sofer Z, Marzari N, Coleman JN, O'Regan DD (2019) Equipartition of energy defines the size-thickness relationship in liquid-exfoliated nanosheets. ACS Nano 13:7050–7061

[35] Zhang JJ, Liu QQ, Ruan YB, Lin S, Wang K, Lu HB (2018) Monolithic crystalline swelling of graphite oxide: a bridge to ultralarge graphene oxide with high scalability. Chem Mater 30:1888–1897

[36] Zhang JL, Yang HJ, Shen GX, Cheng P, Zhang JY, Guo SW (2010) Reduction of graphene oxide vial-ascorbic acid. Chem Commun 46:1112–1114

[37] Bai H, Li C, Wang XL, Shi GQ (2010) On the gelation of graphene oxide. J Phy Chem C 115:5545–5551

[38] Du WC, Wu HG, Chen HW, Xu GC, Li C (2020) Graphene oxide in aqueous and nonaqueous media: dispersion behaviour and solution chemistry. Carbon 158:568–579

[39] Naficy S, Jalili R, Aboutalebi SH, Gorkin Iii RA, Konstantinov K, Innis PC, Spinks GM, Poulin P, Wallace GG (2014) Graphene oxide dispersions: tuning rheology to enable fabrication. Mater Horiz 1:326–331

[40] Lin XY, Shen X, Zheng QB, Yousefi N, Ye L, Mai YW, Kim JK (2012) Fabrication of highly-aligned, conductive, and strong graphene papers using ultralarge graphene oxide sheets. ACS Nano 6:10708–10719

[41] Xu W, Mao N, Zhang J (2013) Graphene: a platform for surface-enhanced raman spectroscopy. Small 9:1206–1224

[42] Eigler S, Dotzer C, Hirsch A (2012) Visualization of defect densities in reduced graphene oxide. Carbon 50:3666–3673

[43] Moon IK, Lee J, Ruoff RS, Lee H (2010) Reduced graphene oxide by chemical graphitization. Nat Commun 1:73